

Article

Effect of Independent Variables on Urban Flood Models

Yanfen Geng ^{*}, Baohang Zhu and Xin Zheng

School of Transportation, Southeast University, Nanjing 211189, China; 220193165@seu.edu.cn (B.Z.); 220162553@seu.edu.cn (X.Z.)

* Correspondence: yfgeng@seu.edu.cn

Received: 18 September 2020; Accepted: 27 November 2020; Published: 8 December 2020



Abstract: The simulation accuracy of urban flood models is affected by independent variables describing terrain resolution and artificial land cover. An evaluation of these effects could provide suggestions for the improvement of simulation accuracy when the available terrain resolutions and representation methods of land cover are different. This paper focused on exploring and evaluating these effects on simulation accuracy using two indicators, relative depth accuracy (RDA) and relative area accuracy (RAA). The study area was the Nanjing Jianye district in China, which has experienced extensive urbanization. Designed rainfall (2 and 10 year return periods) and three terrain resolutions (17, 35, and 70 m) were used in this paper. Building blocks (BB), road drainage (RD), and a combination of both (BB + RD) were compared to present the effect of artificial land cover. Real flood events were initially simulated as a model verification case, and hypothetic modeling scenarios were simulated to evaluate the effects of different resolutions and representation methods. The results indicate that the effect of terrain resolutions on simulation accuracy was more obvious than that of artificial land cover in the study area. In this paper, 20–30% higher accuracy could be achieved in the 35 m resolution model with respect to the 70 m resolution model. A relative accuracy of 94% was achieved in the 17 m resolution model when using the BB method, which was 5% higher than that using the RD method. This paper shows that evaluating the effects of terrain resolution and artificial land cover is effective and helpful for improving the simulation accuracy of urban flood models in extensively urbanized districts.

Keywords: urban flood model; independent variables; terrain resolution; artificial land cover; effect evaluation

1. Introduction

Urban flooding has become a significant issue due to the frequent occurrence of urban storms. More than 60% of the cities in China encountered flooding events in recent years [1]. Many studies were undertaken by researchers in the field of flood disasters [2–5]. Recently, new modeling methods were proposed in attempts at urban flood simulation [6–8]. Urban flood models are widely used as a reliable tool in flood management. High-accuracy flood simulations can effectively help managers to prevent and mitigate urban flood disasters. However, the simulation accuracy of urban flood models is easily affected by independent variables in the process of flood simulation [9], particularly terrain resolution, artificial land cover, and rainfall intensity. Hu et al. [10] previously analyzed 48 peer-reviewed journal articles published between 2015 and 2019 on the Web of Science™ database, studying the impact of rainfall input. Their findings were of great significance for the future development of urban flood models. Studies on the effect of terrain resolution and artificial land cover are also important for an improvement in simulation accuracy.

With regard to terrain resolution, previous studies mostly focused on mountainous and plain areas [11–14]. Recently, the effect of resolution on urban flood models attracted the attention of scholars. Xing et al. [15] recommended that simulations should be performed at resolutions higher than 5 m in hydrodynamic models. However, digital elevation model (DEM) data with a high resolution (finer than 5 m) and detailed information are often rare, unavailable, or expensive, especially for the remote cities of developing countries [16]. Other resolutions (30 m or lower) are more easily available; these models need to be properly evaluated. In order to understand the effect of input resolution on the simulation outcomes, Elaji and Ji [17] simulated urban runoff using different resolutions (3–30 m resolution DEMs with 6–30 m resolution images). Their results proved the good tolerance of their developed simulation approach for small variations in input parameters. However, a quantitative evaluation of this effect needs to be addressed in further work.

A thorough consideration of urban terrain, buildings, roads, water systems, pipe networks, and other factors allows accurately simulating the rainfall runoff process in urban areas [18]. Artificial land cover (e.g., roads and buildings) cannot be ignored due to its non-negligible effect on flooding [19,20]. Some scholars conducted relevant studies using hydrological or hydrodynamic models. Vojinovic et al. [21] explored the effect of different features such as roads and buildings on the simulation results in two-dimensional floodplains. As a function of the theory of early urban flood models, effect analyses of their results were limited. Building representations in different methods were also compared and discussed in urban flood models, such as building block (BB) and building resistance (BR) [22,23]. The BR method was deemed a good choice for urban flood simulations when detailed building geometry data were not available. The BB method was relatively easy to implement and could improve accuracy through the implementation of a relatively fine grid around buildings. The effect of roads was not considered, and the degree of effect on the simulation results was unclear in their urban flood model. Hence, there is a need to apply and evaluate different representation methods of buildings and roads, as well as provide suggestions with respect to appropriate methods in the modeling process.

This paper took the Jianye district, which has experienced extensive urbanization, as the study case; the results confirm the accuracy of the evaluation approach, suggesting its potential use for urban flood models in similar districts. The main aim of this paper was to explore and evaluate model accuracy as a function of terrain resolution and artificial land cover in the study area by establishing several modeling scenarios with varying DEM resolutions (17, 30, and 70 m), land-cover representation methods (BB, road drainage (RD), and BB + RD), and rainfall intensities (2 and 10 year return periods). Furthermore, real flood events were initially simulated as a model verification case, and hypothetical scenarios were simulated and compared. Two indicators were developed to evaluate the accuracy difference: relative depth accuracy (RDA) and relative area accuracy (RAA).

2. Materials and Methods

2.1. Study Area

Jianye district, which has experienced extensive urbanization, is one of the major districts of Nanjing, located in the southwest (Figure 1). Nanjing belongs to the subtropical monsoon climate with abundant rainfall (annual precipitation, 1200 mm). According to rainfall characteristics in Nanjing from 1951 to 2017, the Keifer and Chu rainfall pattern method is recommended [24]. This paper used two return periods (2 and 10 years) with the Urban Drainage Design Specification and Urban Flood Control Design Specification, published by the Ministry of Construction and Ministry of Water Resources in China. Rainfall intensities and total rainfall are shown in Figure 2.

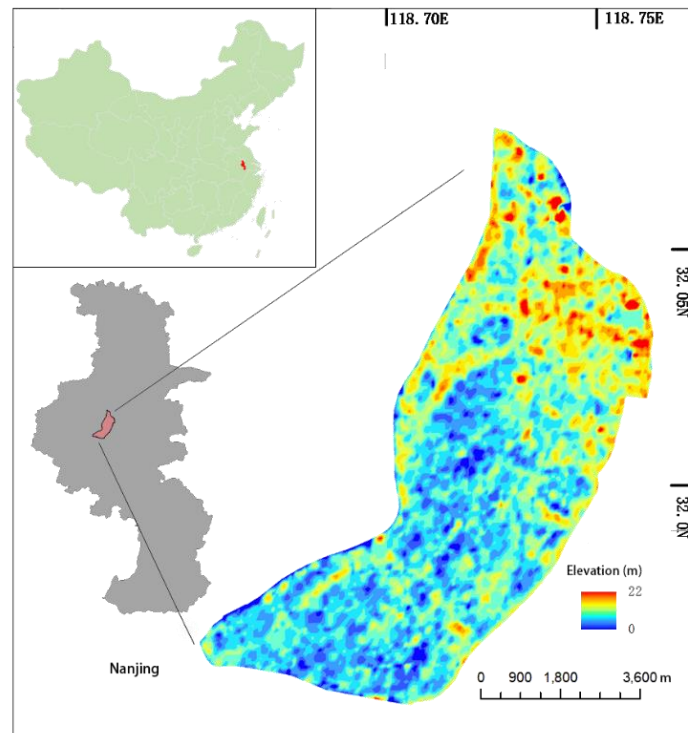


Figure 1. Study area.

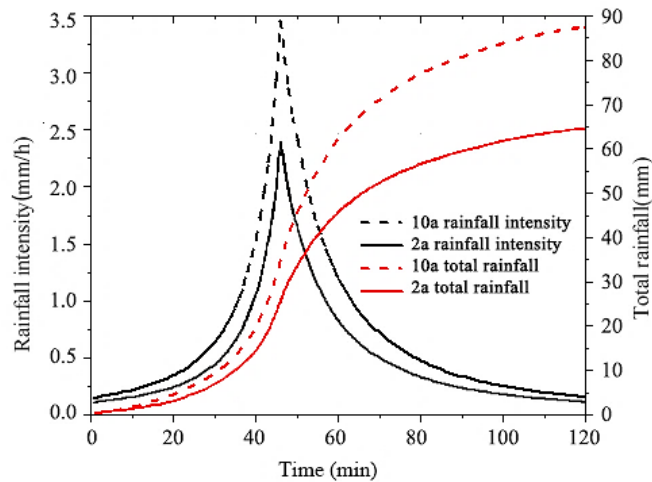


Figure 2. The 2 and 10 year rainfall intensities and total rainfall.

Jianye district is relatively complete and independent, including roads, buildings, green spaces, water systems, and other land cover. It features a flat terrain with a ground elevation of 5.5–7.5 m, as shown in Figure 1. In this paper, three terrain resolutions (17, 35, and 70 m) were resampled on the basis of the ASTER GDEM data collected on the Geospatial Data Cloud platform.

2.2. Methods

2.2.1. Accuracy Evaluation

In order to evaluate the effect of buildings and roads, three representation methods were used: building block (BB), road drainage (RD), and a combination of both (BB + RD). In the first method, buildings appear as blocks, and ground elevation data are raised to heights that cannot be inundated [22]. In the second method, the spatially distributed elevation data of roads are reduced by taking the height

of the kerb as the standard. Hence, roads appear as shallow channels that can affect surface flow in the urban flood model. The BB + RD method simultaneously represents buildings as solid blocks and roads as shallow channels. A total of ten modeling scenarios were developed using various resolutions, representation methods, and rainfall intensities, as shown in Table 1.

Table 1. Modeling scenarios using various resolutions, representation methods, and rainfall intensities.

	Case Number	Terrain Resolution	Representation Method	Rainfall Intensity Return Periods
Reference Cases	C1	17 m	BB + RD	10 years
	C2	17 m	BB + RD	2 years
Contrast Cases	C3	35 m	BB + RD	10 years
	C4	70 m		
	C5	35 m	BB + RD	2 years
	C6	70 m		
	C7	17 m	RD	10 years
	C8		BB	
	C9	17 m	RD	2 years
	C10	17 m	BB	

This paper focused on quantitatively evaluating the effect of terrain resolution and artificial land cover. Table 2 shows the four categories of simulated results encompassing the reference case (RC) and contrast case (CC), where $h_{t,RC}$ is the simulated inundation depth at moment t in the reference case, $h_{t,CC}$ is the simulated inundation depth at moment t in the contrasting cases, $S_{i,RC}$ is the simulated inundation area at inundation depth grade i in the reference case, and $S_{i,CC}$ is the simulated inundation area at inundation depth grade i in the contrasting case.

Table 2. Four categories of the simulated results encompassing the reference case (RC) and contrast case (CC).

Simulation	Categories	
	Inundation Depth (h)	Inundation Area (S)
Reference case (RC)	$h_{t,RC}$	$S_{i,RC}$
Contrast case (CC)	$h_{t,CC}$	$S_{i,CC}$

The relative depth accuracy (RDA) and relative area accuracy (RAA) were used to evaluate the accuracy of modeling results, as defined in Equations (1) and (2), respectively.

$$RDA = 1 - \left| \frac{\sum \left[\left(\sum_{t=1}^T \frac{h_{t,CC} - h_{t,RC}}{h_{t,RC}} \right) / T \right]}{k} \right|, \quad (1)$$

where t is the time (min), T is the duration of rainfall (min), and k is the number of random observation points.

$$RAA = 1 - \left| \left(\sum_{i=1}^m \frac{S_{i,CC} - S_{i,RC}}{S_{i,RC}} \right) / m \right|, \quad (2)$$

where m is the number of inundation depth grades, and i indicates the inundation depth grade.

2.2.2. Hydraulic Model

In this paper, the urban flood model was established by coupling a one-dimensional pipe network model and a two-dimensional surface flow model with the mature MIKE 21 model [25]. The sewer flow in the pipe network was considered as one-dimensional flow, solved by using the

Saint-Venant equations. In a one-dimensional flow regime, it is assumed that the water body is incompressible and homogeneous. The bottom slope of the open channel is small, and the water surface is parallel to the bottom slope (the length was much longer than the inundation depth in this paper: $L/H > 100$). Saint-Venant equations were discretized using the six-point Abbott–Ionescu scheme and solved using the catch-up method. The ADI central difference scheme was used to solve the depth-averaged two-dimensional shallow water equations.

The vertical connection between the one-dimensional pipe network model and the two-dimensional surface flow model was established using a manhole and gutter inlet, whereas the weir flow equation and orifice equation were used to calculate the flow exchange.

3. Model Verification

ASTER GDEM elevation data were resampled to 17 m resolution through data reclassifying and depression filling in ARCGIS software. Road and building elevation data extracted from a satellite image map were merged with the resampled data using the MIKE solver. The terrain distribution map is shown in Figure 3.

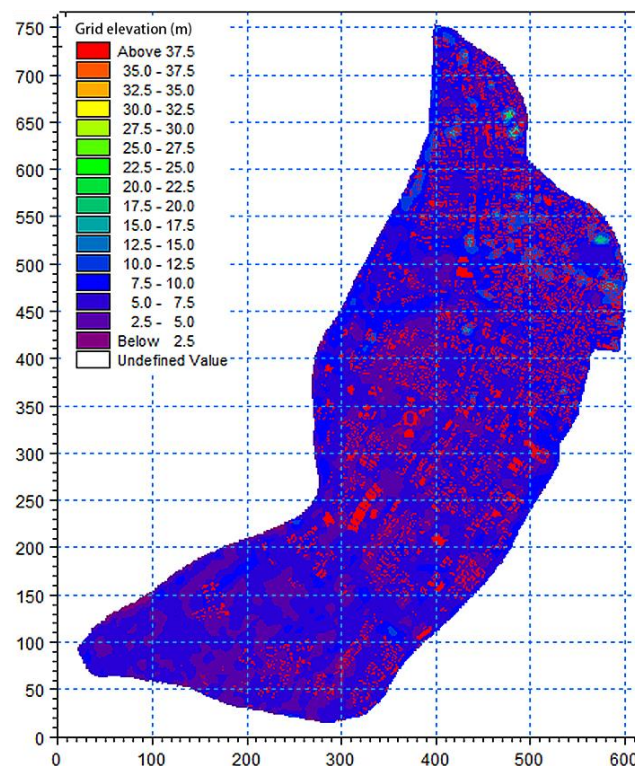


Figure 3. Terrain distribution map of study area.

The water resistance coefficients for different land cover according to the surface condition of the study area and software recommendations were as follows: road, $62.5 \text{ m}^{1/3}/\text{s}$; green space, $25 \text{ m}^{1/3}/\text{s}$; vacant land, $36 \text{ m}^{1/3}/\text{s}$; building, $12.5 \text{ m}^{1/3}/\text{s}$. The remaining parameters were as follows: dry boundary value, 0.002 m; wet boundary value, 0.003 m; eddy viscosity coefficient (E) = $0.1 \times \Delta x^2 / \Delta t$, where Δx is the space interval and Δt is the time step. The model parameters for different spatial resolutions were the same, regardless of the Coriolis force and other source terms.

The pipe network model was established on the basis of the measured data and relevant specifications. The sub-catchment area was divided according to node location using the Tyson polygon method. As shown in Figure 4, the impermeability of sub-catchment areas was obtained according to the runoff coefficients of different surfaces and the area-weighted average. The surface flow model and the pipe network model were coupled through vertical connections at manholes.

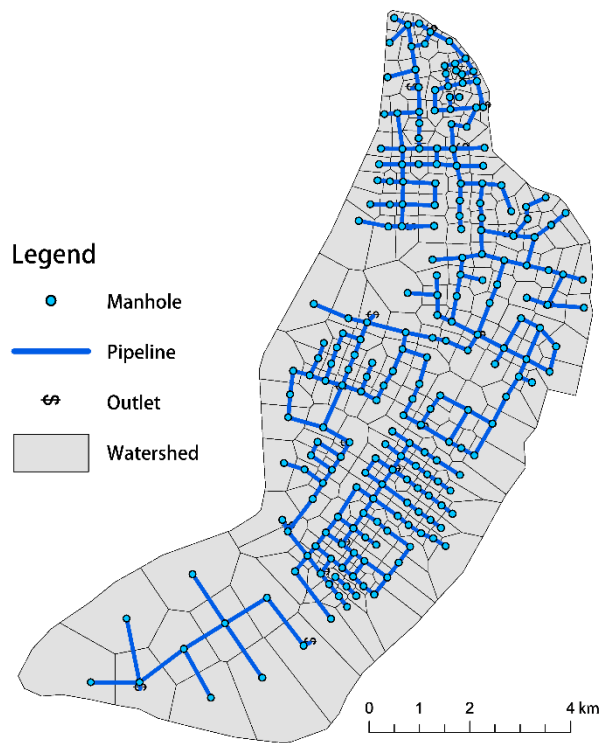


Figure 4. Pipeline network drainage model of study area.

In this paper, a real flood event on 7 August 2017 was simulated using historical rainfall data (Figure 5). The model was tested via an investigation of inundation positions and simulation results. The validation result is shown in Figure 6. Fifteen inundation positions (Table 3) according to previous investigations were verified in the simulation results, thus indicating the good applicability of the established model.

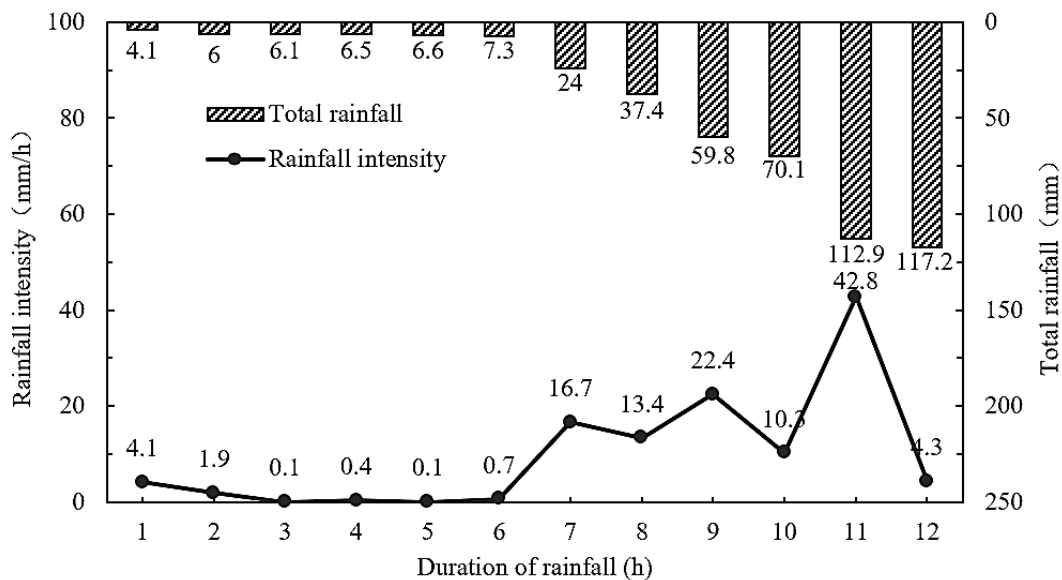


Figure 5. Historical rainfall data in Nanjing on 7 August 2017.

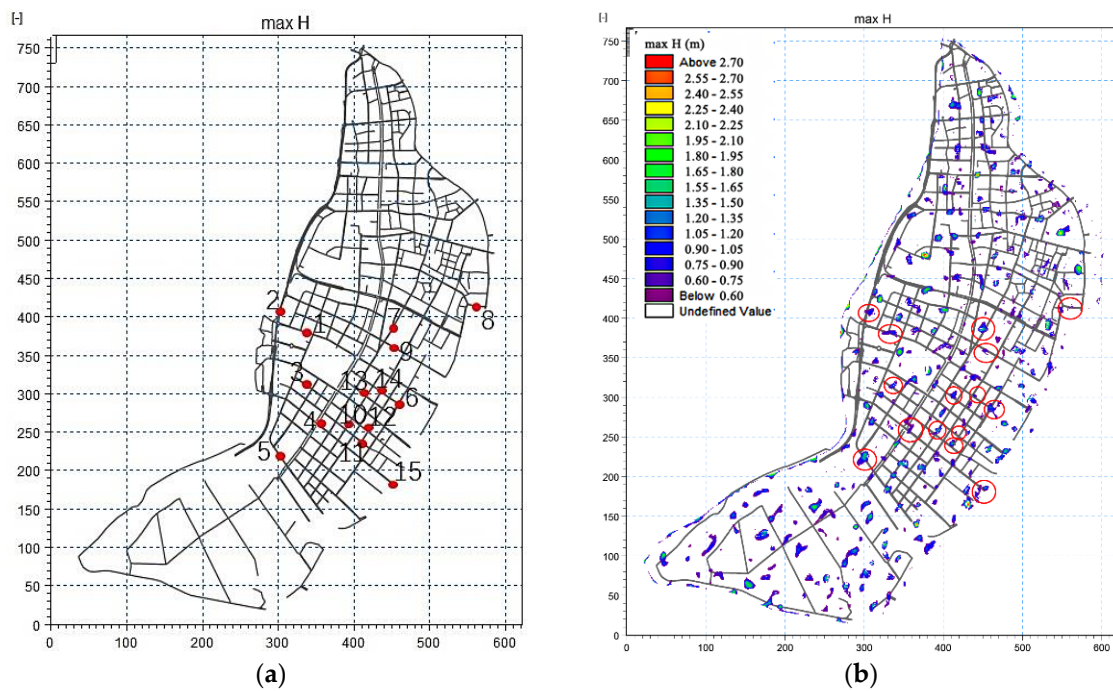


Figure 6. The comparison of investigation records and simulation results: (a) inundation positions according to previous investigations; (b) inundation positions according to simulation.

Table 3. Fifteen inundation positions according to previous investigations in the study area.

No.	Inundation Positions
1	Mengdu street
2	South of Aoti new city tunnel, Yangzi river avenue
3	Fuchunjiang west street Nanxijiang street
4	Bailongjiang street
5	Jinshajiang street
6	Taishan Road
7	Xinglong street
8	Jiqingmen street to Changhong road from west to east
9	Yikang street to Lushan road
10	Hengshan road
11	Songshan road
12	Fuchunjiang street
13	Xin'anjiang street
14	Mudanjiang street
15	Shazhou police station

4. Results and Discussion

4.1. Terrain Resolution Simulation Analysis

The urban flood models of cases C1 to C6 were established. Using the simulation results of cases C1 and C2 as standard data, the inundation areas for cases C3 to C6 were analyzed, as visualized in Figure 7.

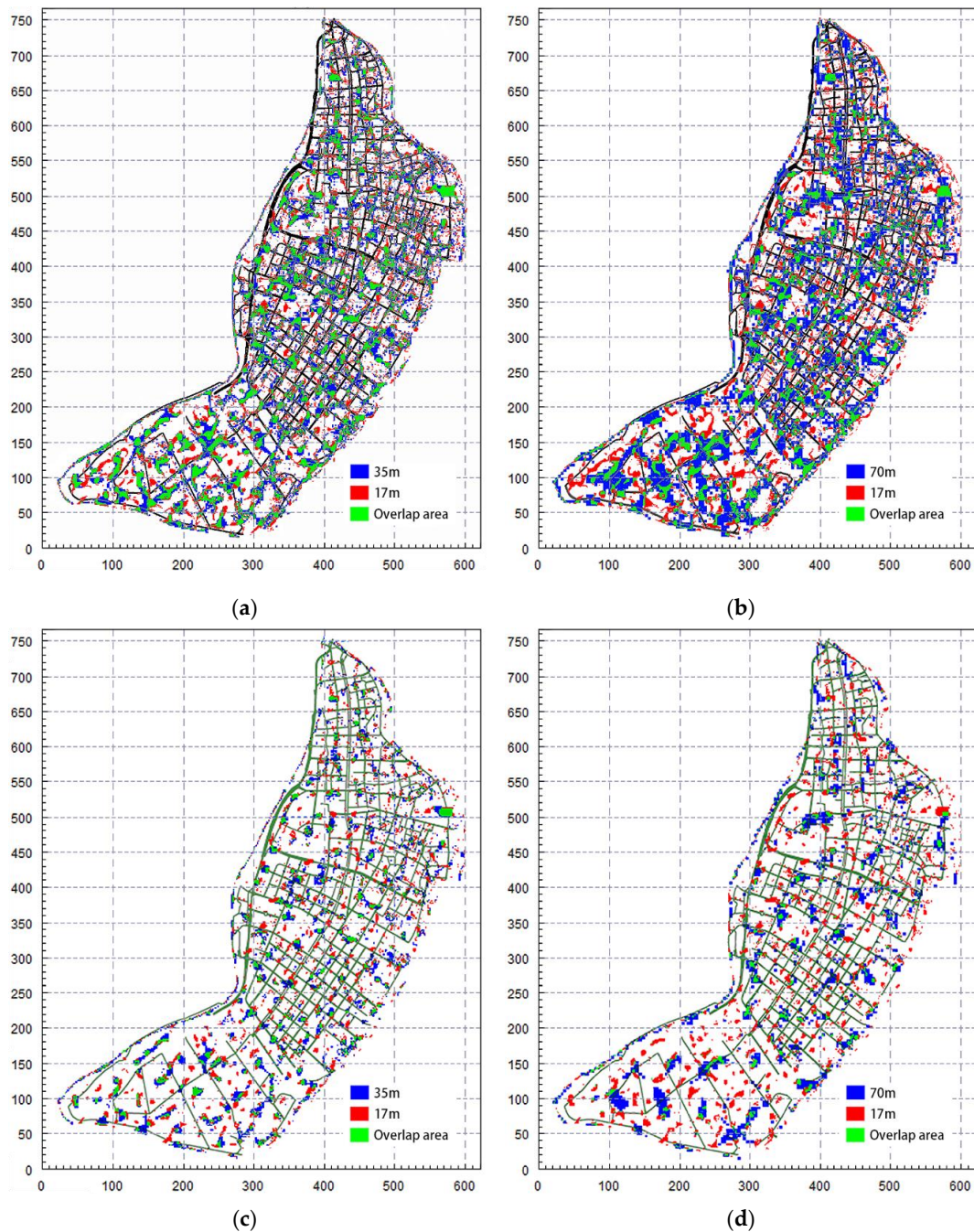


Figure 7. Contrast results of simulated inundation area: (a) cases C1 and C3; (b) cases C1 and C4; (c) cases C2 and C5; (d) cases C2 and C6.

The contrast results under the same rainfall conditions showed that the inundation area at 35 m resolution was highly consistent with the reference data. The contrast results at 70 m resolution presented a relatively large inundation location, and the overlap area with the standard data was small. The inundation area decreased with the improvement in terrain resolution. The distribution of inundation locations along the roads was obvious. As shown in Figure 8, four observation points were observed to analyze the process of inundation depth with time. The depth–time curves of cases C1 to C6 are shown in Figure 9, showing a relatively similar trend for the three terrain resolutions. The trend for the 35 m resolution case was more consistent with the reference case than that for the 70 m resolution case.

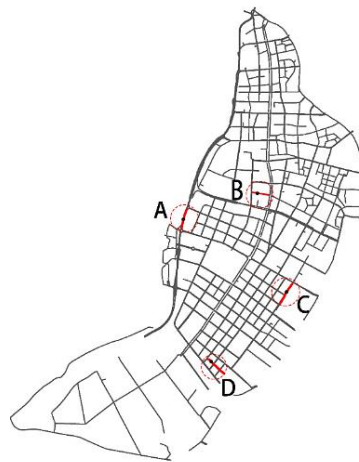


Figure 8. Distribution of observation points in study area.

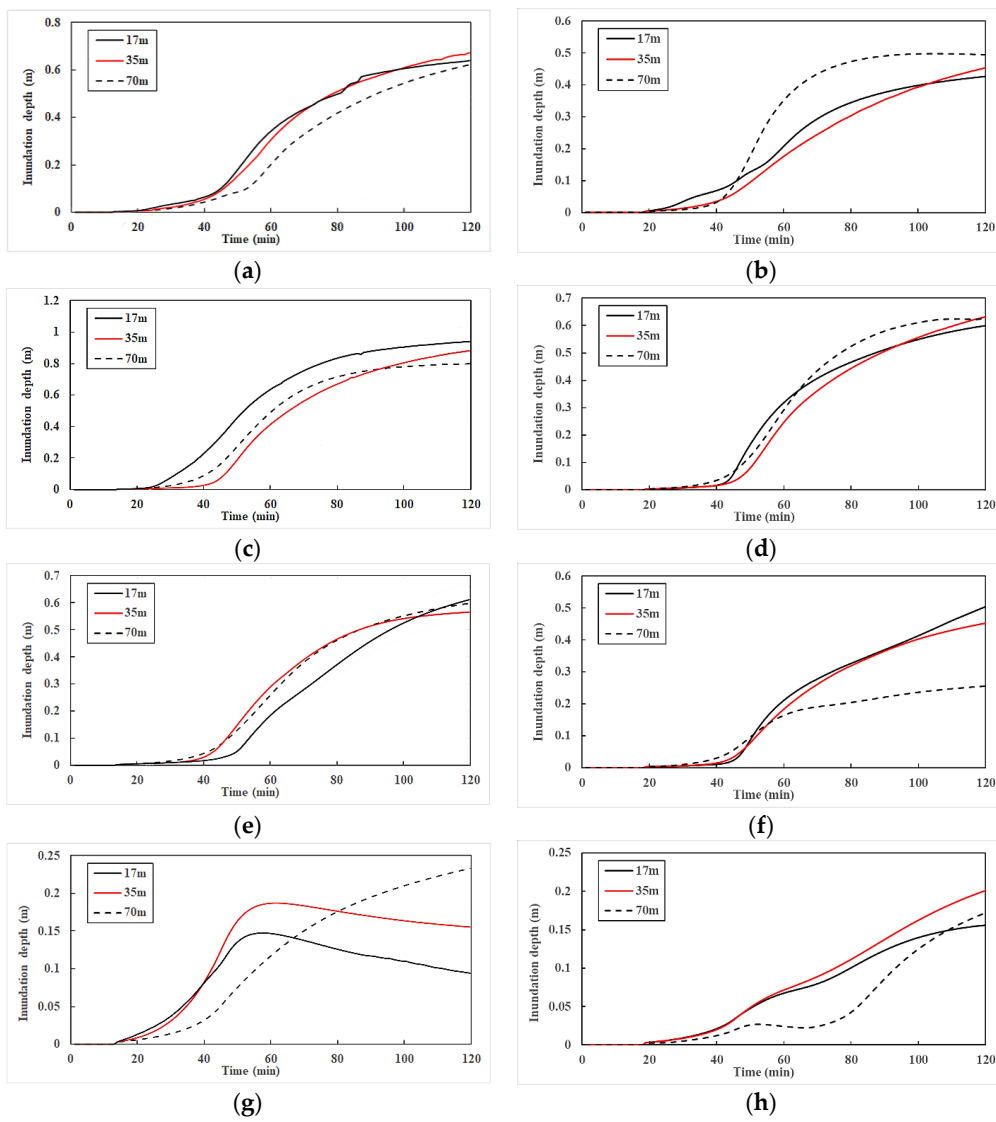


Figure 9. The inundation depth as a function of time for the three terrain resolutions (17, 35, and 70 m) at four observation points: (a,c,e,g) 10-year return period; (b,d,f,h) 2-year return period.

The inundation depth was divided into four grades: 0.05–0.15 m, 0.15–0.3 m, 0.3–0.4 m, and >0.4 m, with the inundation areas calculated for each grade. The results are shown in Figure 10. The total inundation areas for cases C1, C3, and C4 were 13.13 km², 15.02 km², and 19.63 km², respectively. The inundation area for the 70 m resolution case was 30.7% larger than that for the 35 m resolution case and 49.5% larger than that for the 17 m resolution case. The inundation area for the 35 m resolution case was 14.4% larger than that for the 17 m resolution case. The total inundation areas for cases C2, C5, and C6 were 10.35 km², 11.52 km², and 14.35 km², respectively. The inundation area for the 70 m resolution case was 24.5% larger than that for the 35 m resolution case and 38.7% larger than that for the 17 m resolution case. The inundation area of the 35 m resolution case was 11.42% larger than that for the 17 m resolution case. Furthermore, the error for the 35 m resolution case was reduced by approximately 30% with respect to the 70 m resolution case. According to a comprehensive evaluation of the data, the inundation area error was obviously less for the of 35 m resolution case than the 70 m resolution case.

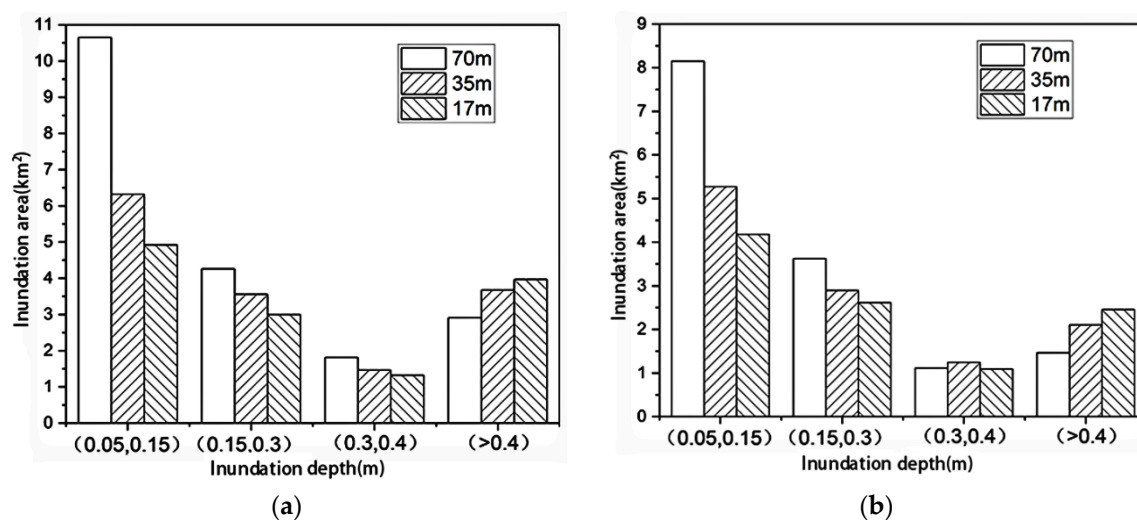


Figure 10. The inundation area for different inundation depths at 17, 35, and 70 m resolutions: (a) 10-year return period; (b) 2-year return period.

4.2. Artificial Land Cover Simulation Analysis

Using the simulation results for cases C1 and C2 as standard data, the effects of artificial land cover for cases C7 to C10 are presented in Figure 11. It can be found that most inundation areas overlapped well, whereas the nonoverlapping areas were located in the middle of the study area and distributed along the road (Figure 11a,b). This was predominantly due to the drainage effects of roads on local shallow surface flow. The nonoverlapping areas were distributed in the north of the study area, where urban buildings were concentrated (Figure 11c,d), as the water resistance of building blocks was not considered.

Figure 12 presents the inundation depth-time curves for the four observation points, showing that the trends were coincident at points A–C. However, there was an obvious anomaly at point D, whereby the turning point of inundation depth was significantly ahead of time when using the RD method. Under a 2-year return period, buildings had a greater effect on surface flow than roads, even affecting the drainage process at local inundation areas. The effect of buildings on the evolution trend in local areas can be helpful in the exploration of local flood and drainage.

Hundreds of locations in the study area were randomly observed to conduct fitting analysis on the maximum inundation depth. As shown in Figure 13, the simulation results using the BB and RD methods matched well with the results using the BB + RD method at points with small inundation depth, but varied at points with large inundation depth. The correlation coefficient (R^2) was used to estimate the similarity of two groups of data in this paper. Under the two rainfall conditions,

cases C1 and C8 ($R^2 = 0.97$) and cases C2 and C10 ($R^2 = 0.922$) were highly similar, as opposed to cases C1 and C7 ($R^2 = 0.70$) and cases C2 and C9 ($R^2 = 0.613$). This indicates that the effect of buildings on shallow water flow was significantly greater than that of roads in the urban flood model. The data distributed along the horizontal axis in Figure 13d indicate that the inundation points were mainly positioned alongside buildings when using the RD method.

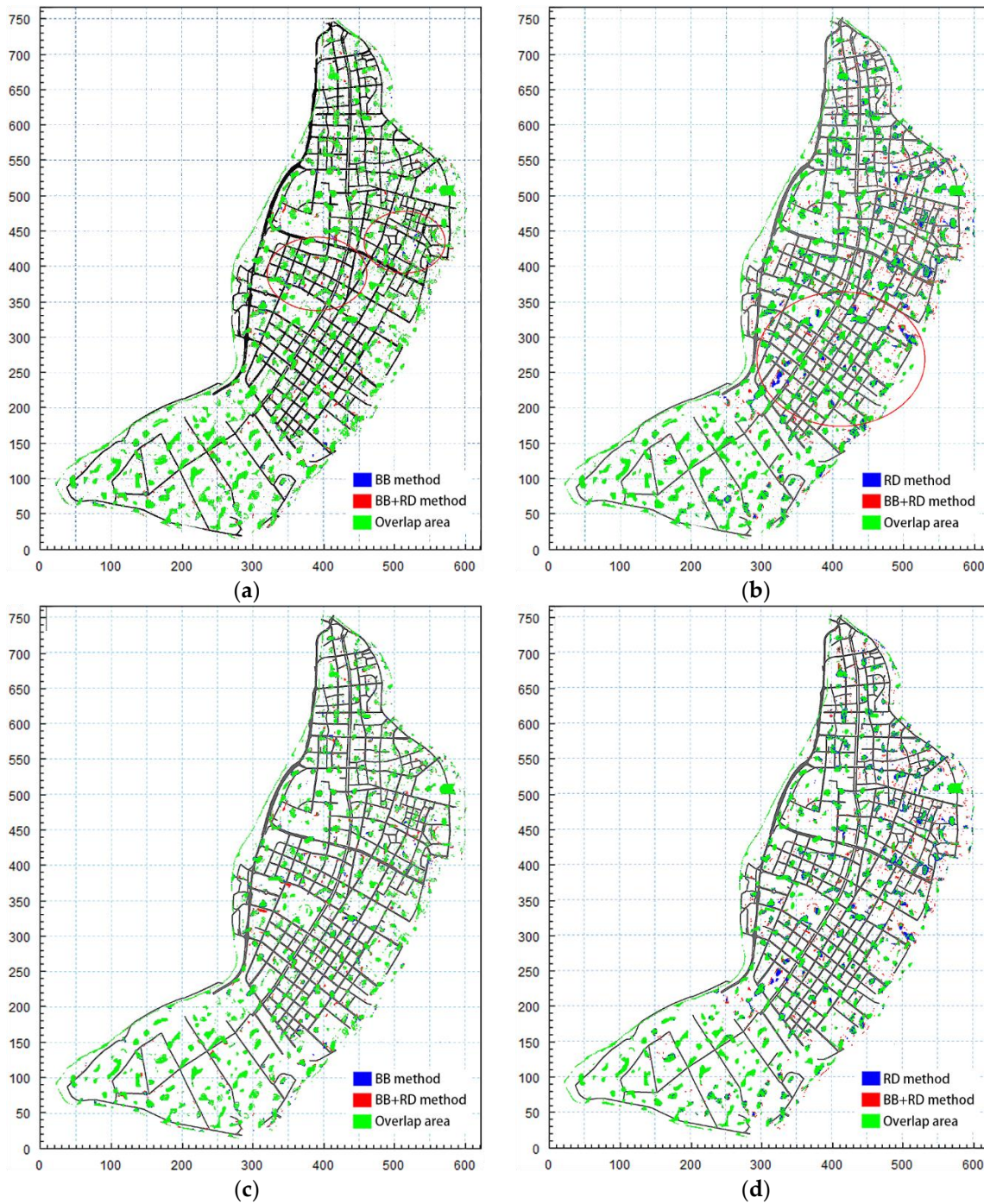


Figure 11. Contrast results for inundation areas when using BB, RD, and BB + RD methods: (a) cases C1 and C8; (b) cases C1 and C7; (c) cases C2 and C10; (d) cases C2 and C9.

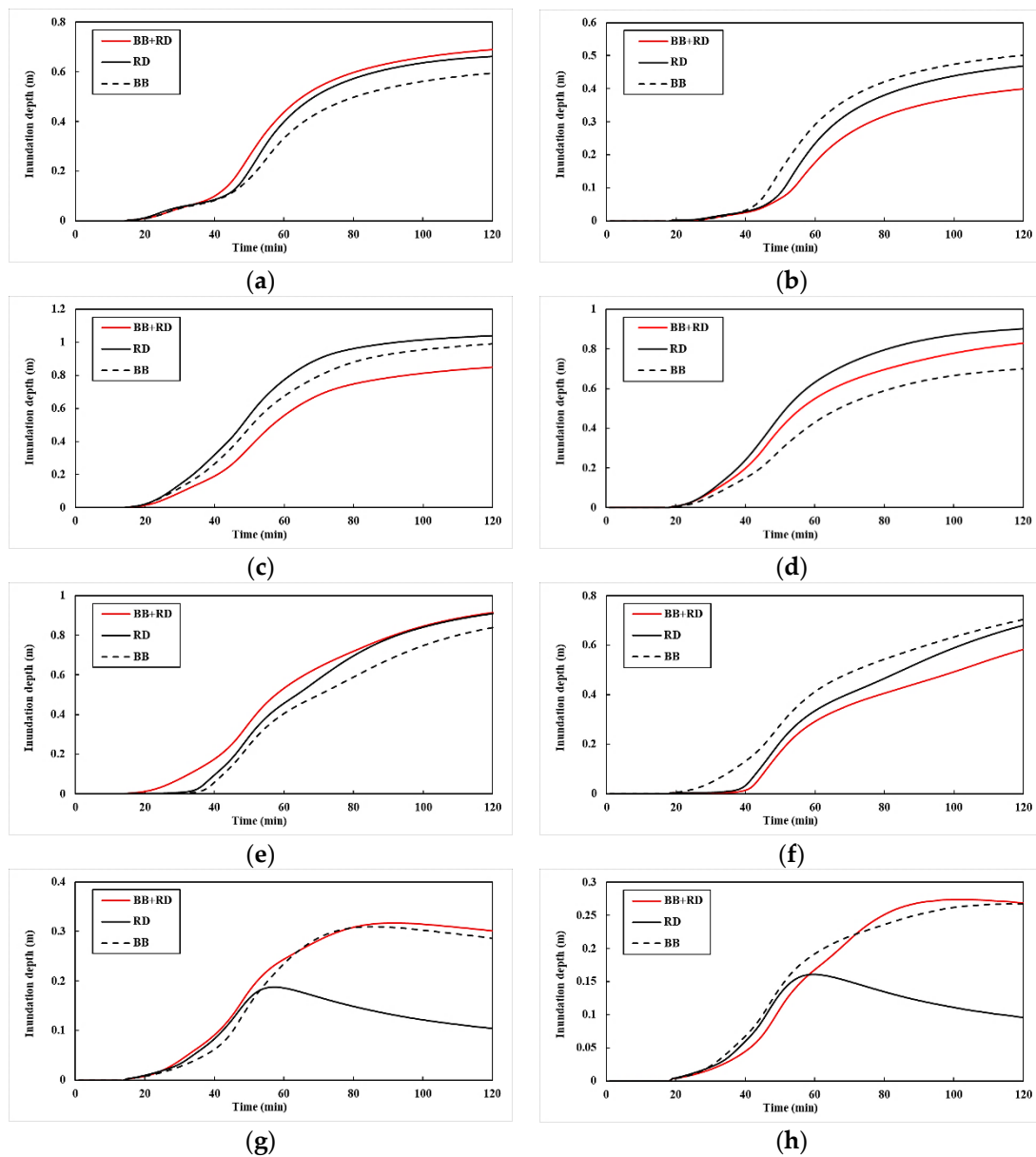


Figure 12. The inundation depth as a function of time when using the BB, RD, and BB + RD methods at four observation points: (a,c,e,g) 10-year return period; (b,d,f,h) 2-year return period.

The statistical results of inundation area are shown in Figure 14. The total inundation areas for cases C1, C7, and C8 were 13.22 km², 13.81 km², and 13.01 km², respectively. The total inundation areas for cases C2, C9, and C10 were 10.34 km², 10.68 km², and 10.14 km², respectively. The inundation area for case C7 was increased by 4.48% with respect to case C1, due to the effect of buildings being ignored. The same phenomenon was observed for case C2 with respect to C9. The observed growth rate was 3.27%. However, the inundation area decreased if the effect of roads was ignored for cases C8 and C10. The growth rates for cases C8 and C10 were −1.57% and −1.94%, respectively, thus indicating that buildings had a greater effect on surface flow than roads.

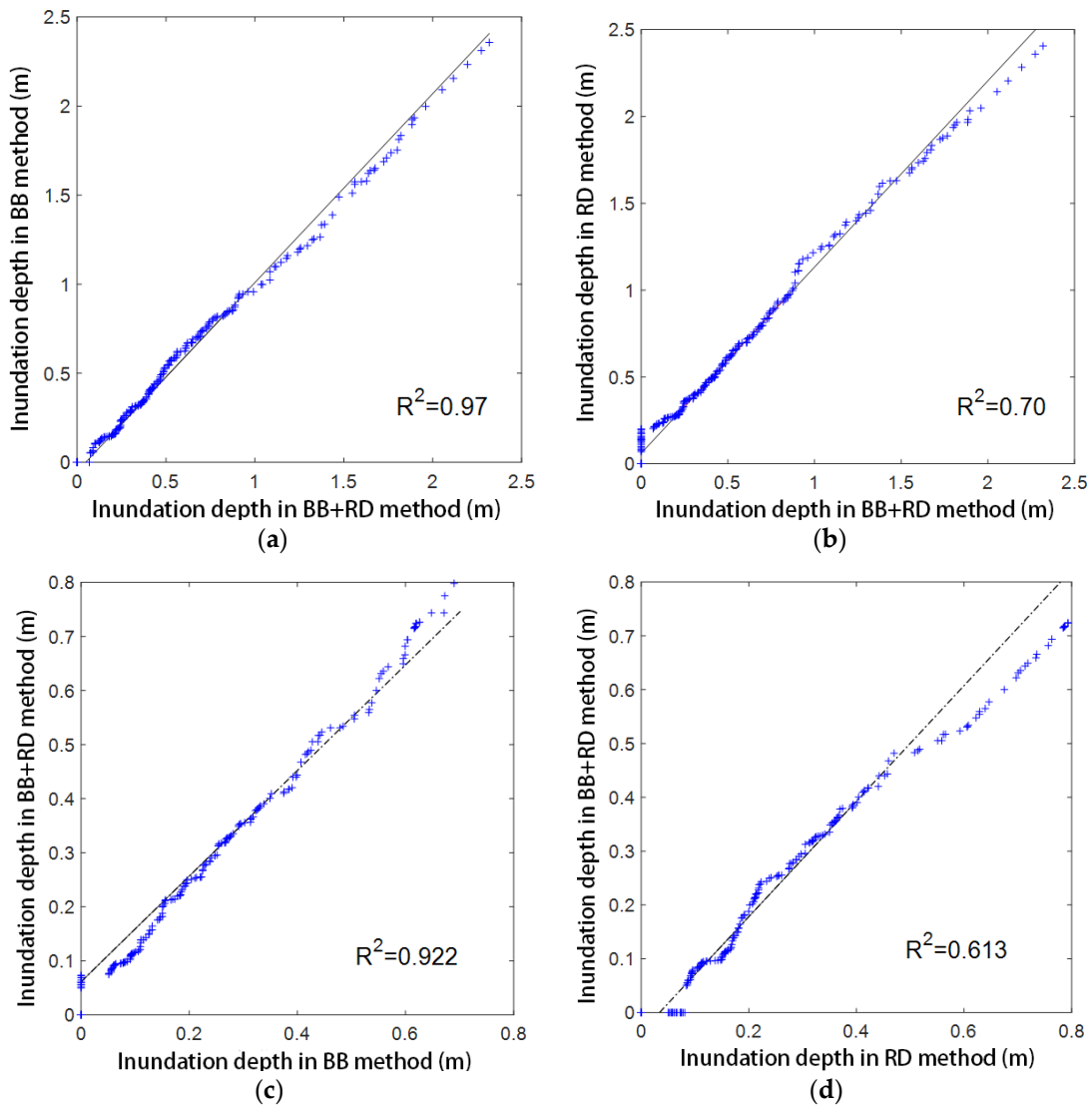


Figure 13. Correlation coefficients (R^2) for maximum inundation depth: (a) cases C1 and C8; (b) cases C1 and C7; (c) cases C2 and C10; (d) cases C2 and C9.

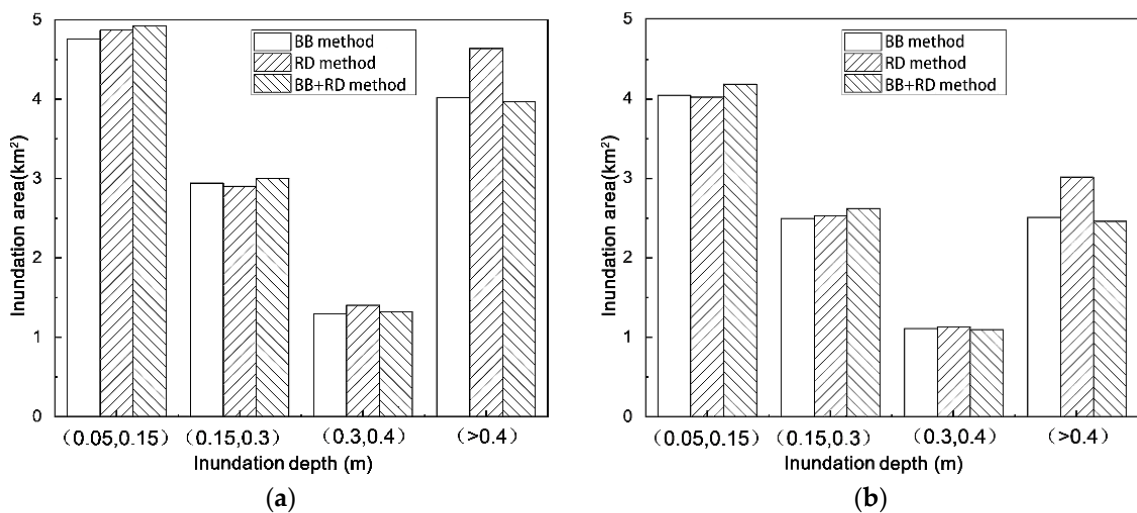


Figure 14. The inundation area as a function of inundation depth when using the BB, RD, and BB + RD methods: (a) 10-year return period; (b) 2-year return period.

4.3. Comparative Analysis of All Simulation Schemes

As can be seen from Table 4 and Figure 15, a reduction in terrain resolution had little effect on the inundation depth, but seriously affected the inundation area under a 2-year rainfall return period. Both inundation depth and inundation area were obviously affected by a decrease in terrain resolution under a 10 year rainfall return period. A lower resolution led to a greater effect on the simulation results. For both rainfall events at 17 m resolution, greater errors were obtained when using the RD method with respect to the BB method.

Table 4. The indicators for all simulated events for different contrast cases. RDA, relative depth accuracy; RAA, relative area accuracy.

Rainfall Return Periods	Indicator	70 m	35 m	17 m	17 m
		BB + RD Method	BB + RD Method	RD Method	BB Method
2 years	RDA	0.9896	0.9942	0.8978	0.9405
	RAA	0.7623	0.9080	0.9538	0.9880
10 years	RDA	0.4905	0.8005	0.9266	0.9700
	RAA	0.5669	0.8632	0.9449	0.9926

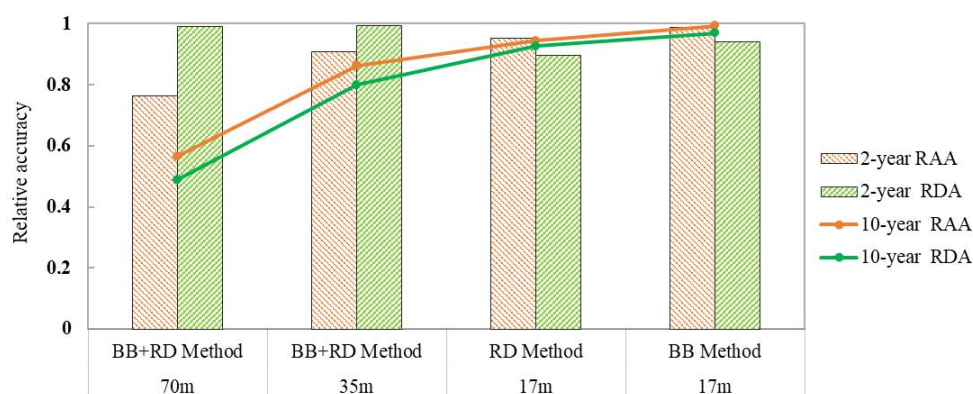


Figure 15. The relative accuracy indicators for all simulation cases.

In addition, the effect of independent variables was evaluated using RDA and RAA indicators (Table 4). The requirements of terrain resolution were substantial compared with artificial land cover in terms of higher simulation accuracy. For inundation depth and inundation area, the relative accuracy could reach above 80% in the 35 m terrain resolution models (20–30% than with the 70 m terrain resolution models). For the 17 m terrain resolution model, the relative accuracy could reach above 94% when considering only the effect of buildings (5% higher than models only considering the effect of roads).

5. Conclusions

This paper took the Jianye district, which has experienced extensive urbanization, as the study area and focused on exploring and evaluating the effect of terrain resolution and artificial land cover on the simulation accuracy of urban flood models. The validated model was used to simulate hypothetic scenarios, which were developed using various resolutions (17, 35, and 70 m), representation methods (BB, RD, and BB + RD), and rainfall intensities (2 and 10 year return periods). RDA and RAA were calculated to evaluate the accuracy difference. Due to the extensive urbanization of the study area, the effect tendencies reflected in the results of this study could be helpful for flood models of similar urban districts. The most important study results based on Jianye district were as follows:

- (1) The 35 m terrain resolution presented good accuracy in terms of the distribution of inundation area and flood evolution. Compared with the 70 m resolution, the error obtained for total inundation area was reduced by about 30% when using the 35 m resolution.

- (2) In terms of representation methods of artificial land cover, the urban flood model using the BB method could better reflect the actual flood evolution than that using the RD method. Compared with the RD method, the correlation (R^2) of the maximum inundation depth increased by about 30% when using the BB method.
- (3) The effect of terrain resolution on simulation accuracy was more obvious than that of artificial land cover. In the models using the BB + RD method, values of RAA and RDA could reach above 80% for the 35 m resolution models (20–30% higher than the 70 m terrain resolution models). In the models using the 17 m terrain resolution, values of RAA and RDA could reach above 94% when considering only the effect of buildings (5% higher than models only considering the effect of roads).

Author Contributions: Conceptualization, Y.G.; methodology, Y.G. and X.Z.; supervision, Y.G.; writing—original draft, B.Z.; writing—review and editing, Y.G. and B.Z. All authors have read and agreed to the published version of the manuscript.

Funding: This research was funded by the National Natural Science Foundation of China (NSFC) (Grant No. 51979040).

Conflicts of Interest: The authors declare no conflict of interest.

References

1. NDRCC, UNDP. *Investigation Report on Risk Management Capability of Urban Flood Disaster*; UNDP: New York, NY, USA, 2017.
2. Mignot, E.; Li, X.; Dewals, B. Experimental Modelling of Urban Flooding: A Review. *J. Hydrol.* **2019**, *568*, 334–342. [[CrossRef](#)]
3. Ahn, J.; Na, Y.; Park, S.W. Development of Two-Dimensional Inundation Modelling Process Using MIKE21 Model. *KSCE J. Civ. Eng.* **2019**, *23*, 3968–3977. [[CrossRef](#)]
4. Geng, Y. Flood Risk Assessment in Quzhou City (China) Using a Coupled Hydrodynamic Model and Fuzzy Comprehensive Evaluation (FCE). *Nat. Hazards* **2020**, *100*, 133–149. [[CrossRef](#)]
5. Zhang, W.; Zhang, X.; Liu, Y.; Tang, W.; Xu, J.; Fu, Z. Assessment of Flood Inundation by Coupled 1D/2D Hydrodynamic Modeling: A Case Study in Mountainous Watersheds along the Coast of Southeast China. *Water* **2020**, *12*, 822. [[CrossRef](#)]
6. Viero, D.P. Modelling Urban Floods Using a Finite Element Staggered Scheme with an Anisotropic Dual Porosity Model. *J. Hydrol.* **2019**, *568*, 247–259. [[CrossRef](#)]
7. Sanders, B.F.; Schubert, J.E. PRIMo: Parallel Raster Inundation Model. *Adv. Water Resour.* **2019**, *126*, 79–95. [[CrossRef](#)]
8. Li, Q.; Liang, Q.; Xia, X. A Novel 1D-2D Coupled Model for Hydrodynamic Simulation of Flows in Drainage Networks. *Adv. Water Resour.* **2020**, *137*, 103519. [[CrossRef](#)]
9. Dottori, F.; Baldassarre, G.D.; Todini, E. Detailed Data Is Welcome, but with a Pinch of Salt: Accuracy, Precision, and Uncertainty in Flood Inundation Modeling. *Water Resour. Res.* **2013**, *49*, 6079–6085. [[CrossRef](#)]
10. Hu, C.; Liu, C.; Yao, Y.; Wu, Q.; Ma, B.; Jian, S. Evaluation of the Impact of Rainfall Inputs on Urban Rainfall Models: A Systematic Review. *Water* **2020**, *12*, 2484. [[CrossRef](#)]
11. Colby, J.D.; Dobson, J.G. Flood Modeling in the Coastal Plains and Mountains: Analysis of Terrain Resolution. *Nat. Hazards Rev.* **2010**, *11*, 19–28. [[CrossRef](#)]
12. Savage, J.T.S.; Pianosi, F.; Bates, P.; Freer, J.; Wagener, T. Quantifying the Importance of Spatial Resolution and Other Factors through Global Sensitivity Analysis of a Flood Inundation Model. *Water Resour. Res.* **2016**, *52*, 9146–9163. [[CrossRef](#)]
13. Fathy, I.; Abd-Elhamid, H.; Zelenakova, M.; Kaposztasova, D. Effect of Topographic Data Accuracy on Watershed Management. *Int. J. Environ. Res. Public Health* **2019**, *16*, 4245. [[CrossRef](#)]
14. Nagaveni, C.; Kumar, K.P.; Ravibabu, M.V. Evaluation of TanDEMx and SRTM DEM on Watershed Simulated Runoff Estimation. *J. Earth Syst. Sci.* **2018**, *128*, 2. [[CrossRef](#)]
15. Xing, Y. City-Scale Hydrodynamic Modelling of Urban Flash Floods: The Issues of Scale and Resolution. *Nat. Hazards* **2019**, *96*, 473–496. [[CrossRef](#)]

16. Shen, J.; Tan, F. Effects of DEM Resolution and Resampling Technique on Building Treatment for Urban Inundation Modeling: A Case Study for the 2016 Flooding of the HUST Campus in Wuhan. *Nat. Hazards* **2020**, *104*, 927–957. [[CrossRef](#)]
17. Elaji, A.; Ji, W. Urban Runoff Simulation: How Do Land Use/Cover Change Patterning and Geospatial Data Quality Impact Model Outcome? *Water* **2020**, *12*, 2715. [[CrossRef](#)]
18. Ying, X.; Wang, S.S.Y. Evaluation of 2D Shallow-Water Model for Spillway Flow with a Complex Geometry. *J. Hydraul. Res.* **2010**, *48*, 265–268. [[CrossRef](#)]
19. Schubert, J.E.; Sanders, B.F.; Smith, M.J.; Wright, N.G. Unstructured Mesh Generation and Landcover-Based Resistance for Hydrodynamic Modeling of Urban Flooding. *Adv. Water Resour.* **2008**, *31*, 1603–1621. [[CrossRef](#)]
20. Paquier, A.; Mignot, E.; Bazin, P.-H. From Hydraulic Modelling to Urban Flood Risk. *Procedia Eng.* **2015**, *115*, 37–44. [[CrossRef](#)]
21. Vojinovic, Z.; Seyoum, S.D.; Mwalwaka, J.M.; Price, R.K. Effects of Model Schematisation, Geometry and Parameter Values on Urban Flood Modelling. *Water Sci. Technol.* **2011**, *63*, 462–467. [[CrossRef](#)]
22. Schubert, J.E.; Sanders, B.F. Building Treatments for Urban Flood Inundation Models and Implications for Predictive Skill and Modeling Efficiency. *Adv. Water Resour.* **2012**, *41*, 49–64. [[CrossRef](#)]
23. Li, Z.; Liu, J.; Mei, C.; Shao, W.; Wang, H.; Yan, D. Comparative Analysis of Building Representations in TELEMAC-2D for Flood Inundation in Idealized Urban Districts. *Water* **2019**, *11*, 1840. [[CrossRef](#)]
24. Zhang, L.; Li, J.; Pei, H.; He, G. Analysis of rainfall patterns of short duration rainstorm in Nanjing. In *Advances in Meteorological Science and Technology*; China Meteorological Administration Training Center: Beijing, China, 2019; Volume 9, p. 3.
25. Nigussie, T.A.; Altunkaynak, A. Modeling the effect of urbanization on flood risk in Ayamama Watershed, Istanbul, Turkey, using the MIKE 21 FM model. *Nat. Hazards* **2019**, *99*, 1031–1047. [[CrossRef](#)]

Publisher's Note: MDPI stays neutral with regard to jurisdictional claims in published maps and institutional affiliations.



© 2020 by the authors. Licensee MDPI, Basel, Switzerland. This article is an open access article distributed under the terms and conditions of the Creative Commons Attribution (CC BY) license (<http://creativecommons.org/licenses/by/4.0/>).